

LGGNet: Learning from Local-Global-Graph Representations for Brain-Computer Interface

Yi Ding, *Student Member, IEEE*, Neethu Robinson, *Member, IEEE*, Qiuhan Zeng,
and Cuntai Guan, *Fellow, IEEE*

Abstract—Neuropsychological studies suggest that co-operative activities among different brain functional areas drive high-level cognitive processes. To learn the brain activities within and among different functional areas of the brain, we propose LGGNet, a novel neurologically inspired graph neural network, to learn local-global-graph representations of electroencephalography (EEG) for Brain-Computer Interface (BCI). The input layer of LGGNet comprises a series of temporal convolutions with multi-scale 1D convolutional kernels and kernel-level attentive fusion. It captures temporal dynamics of EEG which then serves as input to the proposed local and global graph-filtering layers. Using a defined neurophysiologically meaningful set of local and global graphs, LGGNet models the complex relations within and among functional areas of the brain. Under the robust nested cross-validation settings, the proposed method is evaluated on three publicly available datasets for four types of cognitive classification tasks, namely, the attention, fatigue, emotion, and preference classification tasks. LGGNet is compared with state-of-the-art methods, such as DeepConvNet, EEGNet, R2G-STNN, TSception, and HRNN. The results show that LGGNet outperforms these methods, and the improvements are statistically significant ($p < 0.05$) in most cases. The results show that bringing neuroscience prior knowledge into neural network design yields an improvement of classification performance. The source code can be found at: <https://github.com/yi-ding-cs/LGG>

Index Terms—Deep learning, electroencephalography, graph convolutional neural networks.

I. INTRODUCTION

BRAIN-computer interface (BCI) enables the brain to communicate with machines directly using Electroencephalography (EEG) [1]. A typical BCI system consists of a data acquisition module, a pre-processing module, a classification module, and a feedback module [2]. BCI has a wide range of applications in the real world, such as robot controlling [3], stroke rehabilitation [4], and emotion regulation for mental disorders [5][6].

Compared with traditional machine learning methods [7][8][9][10], deep learning methods achieved superior performances in different tasks of BCI, such as classification of motor imagery [11][12][13][14], mental attention classification [15][16][17], emotion recognition [18][19][20][21], and mental workload detection [22]. However, there is still room to explore neurophysiologically meaningful networks. Delvign *et al.* [16] proposed a Hierarchical Recurrent Neural

Yi Ding, Neethu Robinson, Qiuhan Zeng, and Cuntai Guan are with the School of Computer Science and Engineering, Nanyang Technological University, 50 Nanyang Avenue, Singapore, 639798. e-mail: (ding.yi, nrobinson, qiuhan.zeng, ctguan)@ntu.edu.sg.

Cuntai Guan is the Corresponding Author.

Network (HRNN) that utilized recurrent neural networks to learn from the graph-structured EEG features for attention state classification. Li *et al.* [19] transfer the differential entropy (DE) features of EEG into 2D images according to the relative locations of EEG channels and a Hierarchical Convolutional Neural Networks (HCNN) was designed to extract the spatial pattern of the EEG signals. Although many machine/deep learning methods have been proposed in the BCI domain, most of them highly rely on manually extracted EEG features. With the feature extracting ability of Convolutional Neural Networks (CNNs), directly learning from EEG becomes reliable. Schirrmeister *et al.* [11] proposed deep and shallow convolutional neural networks, named DeepConvNet and ShallowConvNet, to process EEG data. Lawhern *et al.* [14] proposed a compact deep learning framework, EEGNet, that uses three 1D CNN layers to extract the temporal and spatial patterns from EEG. Ding *et al.* [21] designed TSception that utilizes multi-scale convolutional kernels to learn discriminative representations from affective EEG signals. There are mainly two types of information to be learned in EEG data, temporal and spatial information. The temporal information is well studied by the 1D CNNs [11][14] and multi-scale CNNs [21], while the spatial information is not learned effectively.

The brain is a complex network with a hierarchical spatial and functional organization at the level of neurons, local circuits, and functional areas [23]. A commonly used definition of functional areas is the frontal lobe, parietal lobe, temporal lobe, and occipital lobe [18]. Different functional areas correlate to certain brain functions while not working independently. [24]. Neuroscience research [25] suggests that high-order cognitive processes interplay more basic processes such as the ones in attentional, perceptual, and mnemonic systems. And these processes are not unique to the high-order cognitive process, such as emotion. Activating one particular brain region also tends to activate other regions in the group [25]. 1D convolutional kernels along the spatial dimension of EEG [11][14][26] might not be able to capture the complex relations within and among different brain functional areas. Although TSception uses hemisphere kernels to learn the relations between hemispheres, the relations among different functional areas of the brain are not extracted effectively.

To address the above problems, we propose the use of graph representations of EEG to define interconnections within and among brain functional areas. EEG signals can be naturally regarded as graph-structured data, with each electrode being the node and spatial relations or functional connections being the edges. We propose to define the EEG data as a local-global

graph whose local graphs belong to the different functional areas of the brain according to neurological knowledge [23][27]. The nodes in each local graph are fully connected because they reflect the brain activities within each brain functional area. The edges of local graphs, or the global connections among local graphs, reflect the complex functional connections among different brain functional regions. To extract more information-rich representations from EEG as the node attributes in the proposed local-global-graph representations of EEG, a temporal convolutional layer with multi-scale 1D convolutional kernels is adopted [21]. A kernel-level attentive fusion layer is further designed to fuse the learned temporal representations with attention. For graph connection learning, a local graph-filtering layer and a global graph-filtering layer are proposed to learn the brain activities within and among different local graphs. In the local graph-filtering layer, the attributes of the nodes are attentively aggregated into one hidden embedding which represents the activity of the local graph. For the global graph-filtering layer, an instance-specific similarity matrix is proposed as the base adjacent matrix of the global graph. Inspired by DGCNN [28], which utilizes a learnable adjacent matrix in the graph convolutional layer, a learnable adjacent mask is further utilized to select the global connections attentively via back-propagation during the training process. We propose 3 different graph definitions of EEG based on neurophysiological evidence of associations among brain areas for different mental tasks. First, we define the general local-global graph according to the 10-20 system that groups the electrode based on the location of electrodes on functional areas [18]. According to psychophysiological evidence [27], the left and right halves of the human frontal brain areas are differentially associated with particular emotions. Incorporating this, secondly, we define a frontal local-global graph. In this, the frontal region is further divided into smaller local regions which are symmetrically located on the left and right hemispheres to learn more emotion-related local-global representations. Thirdly, a hemisphere local-global graph that has symmetrically located subgraphs in all the functional areas is further adapted to study the effect of the different graph definitions. In this paper, we propose Local- Global-Graph Network (LGGNet) that integrates all the aforementioned learning blocks to model the activities within and among brain functional areas for mental state classification.

To evaluate how LGGNet learns from the local-global-graph representations of EEG, we conducted four different classification tasks on three publicly available benchmark datasets, the attention dataset [29] for cognitive attention classification, the fatigue dataset [30] for mental fatigue classification, and the DEAP dataset[31] for emotion and preference classification, respectively. The proposed LGGNet was compared with several state-of-the-art (SOTA) methods in the BCI domain, namely DeepConvNet (2017) [11], EEGNet (2018) [14], R2G-STNN (2019) [32], TSception (2020) [21], HRNN (2021) [17]. From the experiment results, LGGNet achieved the highest accuracies and F1 scores among the compared SOTA methods in most of the classification experiments. Furthermore, ablation studies were conducted to understand the importance of kernel-level attentive fusion, local and global

graph-filtering layers in LGGNet. To evaluate the effectiveness of involving neuroscientific prior knowledge in LGGNet, the effect of building EEG as local-global graphs as well as the differences among different graph definitions were analyzed. After that, extensive visualization experiments were conducted to better understand what the network learns from EEG. The most informative region of the data identified by the network was visualized using saliency maps [33]. The learned adjacent matrixes for different cognitive tasks were visualized as well.

The major contribution of this work can be summarised as:

- Proposed LGGNet, a neurologically inspired graph neural network, to learn the brain activities within and among different brain functional areas.
- Three different types of local-global graphs, namely the general, frontal, and hemisphere local-global graphs, were proposed to study the effects of different graph definitions on different cognitive tasks.
- The proposed method was compared with several state-of-the-art methods in the BCI field, DeepConvNet (2017) [11], EEGNet (2018) [14], R2G-STNN (2019) [32], TSception (2020) [21], HRNN (2021) [17], on three publicly available datasets for four different types of cognitive tasks: attention, fatigue, emotion, and preference classification.
- Extensive ablation studies and analysis experiments were conducted to better understand LGGNet.

The PyTorch implementation of LGGNet is available at: <https://github.com/yi-ding-cs/LGG>

The remainder of this article is organized as follows. Some related work is given in Section II. In Section III, the proposed LGGNet is introduced. In Section IV, the dataset and experiment settings are presented. The result and discussion are provided in Section V. Finally, we conclude the paper in Section VI.

II. RELATED WORK

A. Different Representations of EEG Data

EEG data have two dimensions: channels (EEG electrodes) and time. The channel dimension reflects the brain activities across different functional areas due to different locations of electrodes on the surface of the human's head. The channel refers to the EEG electrodes if not specified. The time dimension contains the changes in brain activities over time. There are three types of EEG representations commonly used in recent studies, namely 2D time-series, images, and graphs.

The 2D time-series representation is the most commonly used format. For this representation, the network input layer typically consists of temporal convolutional layers to extract temporal information channel by channel and spatial convolutional layers to extract spatial information. Schirrmeister *et al.* [11] proposed deep and shallow convolutional neural networks, named DeepConvNet and ShallowConvNet, to process EEG data. Robinson *et al.* [34] designed a CNN framework to decode hand motor imagery from EEG. Lawhern *et al.* [14] designed EEGNet, which extracts spatial information by the depth-wise 1D convolution kernels. The size of the 1D kernel

is $(n, 1)$, where n equals the number of channels. Hence, the global spatial dependency can be learned.

Another type of EEG representation is the image. In this, the electrodes are rearranged into a 2D frame based on their relative locations on the brain surface, and the raw data or features of each electrode will be the third dimension of the 2D map. Li *et al.* [19] used the relative locations of the electrodes to rearrange the channel dimension of EEG to map each channel on a sparse 2D location map. Siddharth *et al.* [35] applied pre-trained VGG-16 on the EEG-PSD image-based deep learning features for emotion recognition tasks. These image-like representations can reflect the spatial pattern of the EEG. Hence, (n, n) sized convolutional kernels can be applied as the typical convolution on images. The local spatial patterns are captured through sharing kernels. However, one of the drawbacks is that the global spatial information is not well extracted since n is usually small, reducing the perception range.

Recently, many studies have represented EEG data as graphs. In these studies, EEG signals are treated as graphs, with the electrodes being the node and spatial distance or correlations being the edges. Song *et al.* [28] designed dynamic graph convolutional neural networks for EEG emotion recognition with a trainable adjacency matrix. Jang *et al.* [36] defined the connections as both spatial locations and correlations among electrodes to do video classification via EEG graphs. Zhong *et al.* [37] defined the adjacency matrix according to the spatial distance and added some global connections according to asymmetry in neuronal activities.

B. Graph Convolutional Neural Networks

A graph is represented as $\mathcal{G} = (\mathcal{V}, \mathcal{E})$, where \mathcal{V} is the set of nodes, and \mathcal{E} is the set of edges. $v_i \in \mathcal{V}$ denotes a node, and $e_{i,j} = (v_i, v_j) \in \mathcal{E}$ denotes an edge. The adjacency matrix A is derived as an $n \times n$ matrix with $A_{i,j} = 1$ if $e_{i,j} \in \mathcal{E}$ and $A_{i,j} = 0$ if $e_{i,j} \notin \mathcal{E}$. A graph, also known as attributed graph, may have node attributes X , where $X \in \mathbb{R}^{n \times d}$ is a node feature matrix with $\mathbf{x}_v \in \mathbb{R}^d$ representing the feature vector of a node v . A graph can be a directed graph or an undirected one. The adjacency matrix of a directed graph may not be asymmetric if a single-direction connection exists. (e.g., $e_{i,j} \neq e_{j,i}$). The adjacency matrix of an undirected graph is symmetric, and $A = A^T$. Graph Neural Networks (GNNs) [38] were proposed to deal with the graph-structured data. Graph Convolutional Neural Networks (GCNN) [39] extended the convolution operation to graph in the spectral domain. It can generate a node representation by aggregating its features and neighbors' features. Kipf *et al.* [40] proposed a scalable graph convolution neural network, which can encode both local graph structure and the feature of the node with improved computational efficiency.

III. LGGNET FOR BCI

In this section, LGGNet is introduced. Table I illustrates the notations used in this paper. As shown in Fig. 1, LGGNet has three main functional blocks, a temporal learning block, a graph building block, and a graph learning block. The temporal

TABLE I
NOTATIONS USED IN THIS PAPER

Symbol	Description
f_S	sampling rate
α	ratio coefficient of temporal kernel size
k, K	index and number of temporal kernel levels
S_T^k	temporal kernel size
X_n	EEG samples
i	index of EEG samples
c	number of EEG channels
l	length of the EEG sample in time dimension
$\Phi(\cdot)$	activation functions
Z	output tensor of a neural network layer
f	length of features
t	number of T kernels
$\mathcal{F}(\cdot)$	operations
$\Gamma(\cdot)$	concatenation of tensors
$\mathcal{G}_g, \mathcal{G}_f, \mathcal{G}_h,$	general, frontal, and hemisphere graphs
j	index of EEG channels
A_{local}, A_{global}	local and global adjacent matrix
h_{local}	latent representations of local graphs
r, R	index and total number of local graphs
\cdot	dot product
M	trainable attentive mask of global adjacent matrix
w	trainable weight
\circ	Hadamard product
W	trainable weight matrix
b	trainable bias vector
p, P	index and number of nodes in a local graph
\tilde{D}	Degree matrix of the adjacent matrix
m	index of GCN layers
h	length of the hidden output of GCN layers
$\Upsilon(\cdot)$	flatten operation

The order of the symbols is the same as their appearance sequence

convolutional layer in the temporal learning block aims to learn dynamic temporal/frequency representations from EEG directly instead of manually extracted features. In the graph building block, the local-global graph is constructed whose nodes, node attributes, and adjacent connections are EEG channels, the attentively fused temporal representations, and the neuroscience-inspired structures. The graph learning block contains two layers, namely the local and global graph-filtering layers. The local graph-filtering layer learns the brain activities within each local region, after which the global graph-filtering layer with a similarity-based trainable adjacency matrix will be applied to learn complex relations among different local regions.

A. Temporal Learning Block

Temporal learning block has a temporal convolutional layer which is designed to learn dynamic temporal information from the EEG signal of each electrode. The multi-scale temporal convolutional layer utilizes parallel multi-scale 1D temporal kernels (T kernels). In order to learn dynamic-frequency representations, the length of the temporal kernels is set in different ratios of the sampling rate f_S [21]. The ratio coefficient is denoted as $\alpha^k \in \mathbb{R}$, where k is the level of the temporal convolutional layer. k will vary from 1 to K ($\alpha = 0.5, K = 3$, in our study). Hence, the size of T kernels in k -th level, denoted by S_T^k , can be defined as:

$$S_T^k = (1, \alpha^k \cdot f_S), k \in [1, 2, 3] \quad (1)$$

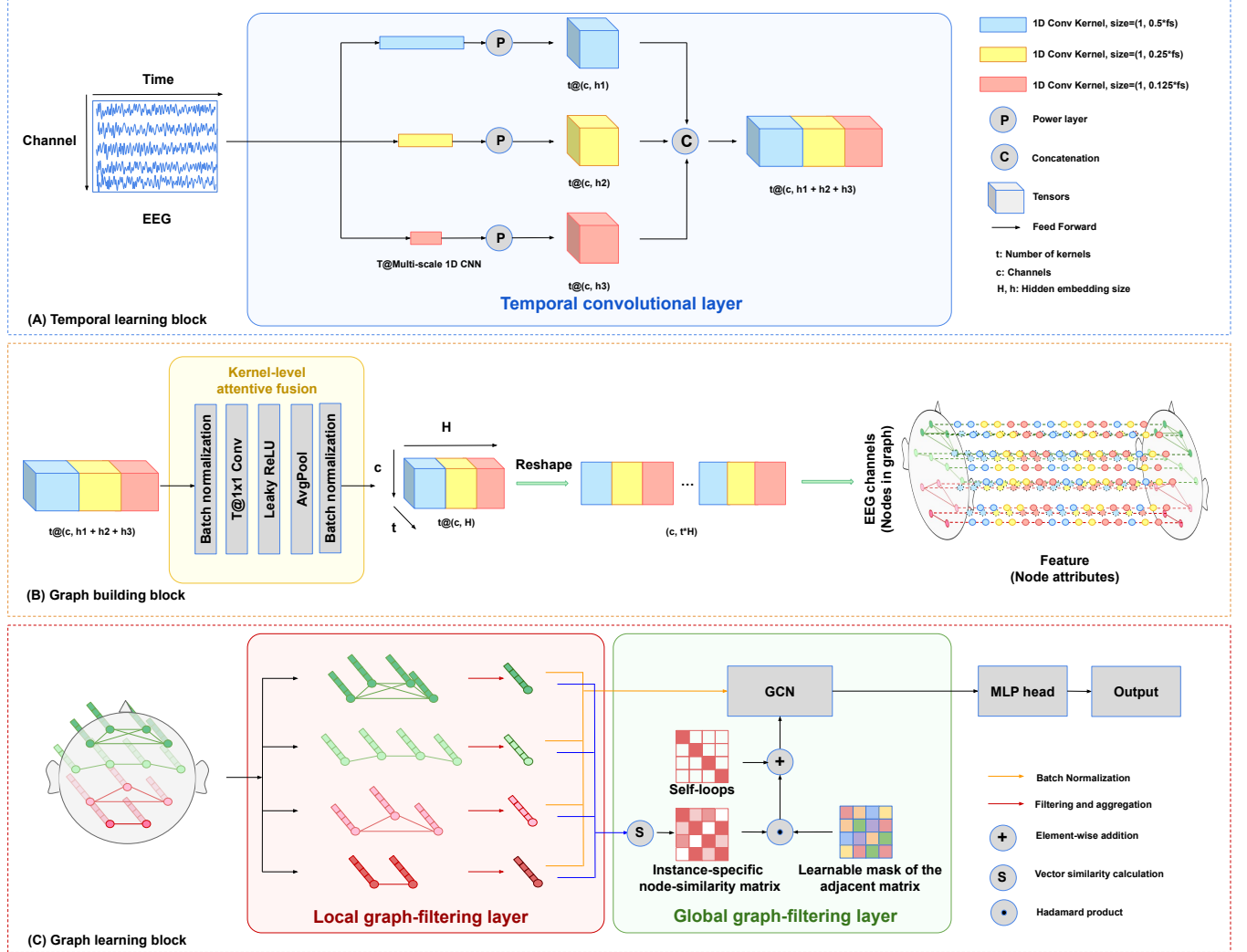


Fig. 1. Structure of LGGNet. LGGNet has three main functional blocks, the temporal learning block, the graph building block, and the graph learning block. The temporal convolutional layer is shown in the temporal learning block (a). Building the local-global graphs of EEG using the attentively fused temporal representations is illustrated in the graph building block (b). The local and global graph-filtering layers are shown in the graph learning block (c). The temporal convolutional layer aims to learn dynamic temporal representations from EEG directly instead of human extracted features. The kernel-level attentive fusion layer will fuse the information learned by different temporal kernels to increase the learning capacity of LGGNet. The local graph-filtering layer learns the brain activities within each local region. Then the global graph-filtering layer with a trainable adjacency matrix will be applied to learn complex relations among different local regions. Four local graphs are shown in the figure for illustration purposes only, the detailed local-global-graph definitions are provided in subsection ‘Local-Global-Graph Representation of EEG’ of section III. Best viewed in color.

The mental state specific information of EEG signals can be reflected in distinct frequency bands [7]. Multi-scale 1D temporal convolutional kernels can enrich the learned dynamic time-frequency representations of EEG [21].

Given the preprocessed EEG data $X_i \in \mathbb{R}^{c \times l}, i \in [1, \dots, n]$, where n equals the number of EEG samples, c is the EEG channel number, and l is the sample length in the time dimension, three multi-scale temporal kernels are applied parallelly to learn dynamic temporal/frequency representations. Instead of using $\Phi_{ReLU}(\cdot)$ [21], we use the logarithmic of the average pooled square of the representations [11] to learn the power features, which are well-studied EEG features in the BCI domain. Let $Z_{temporal}^k \in \mathbb{R}^{t \times c \times f_k}$ denote the output of the k -th level temporal kernel, where t is the number of the T kernels, c is channel number, f_k is the feature length.

$Z_{temporal}^k$ is defined as:

$$Z_{temporal}^k = \Phi_{log}(\mathcal{F}_{AvgPool}(\Phi_{square}(\mathcal{F}_{Conv1D}(X_i, S_T^k)))) \quad (2)$$

where $\mathcal{F}_{Conv1D}(X_i, S_T^k)$ is the convolution operation using T kernel of size S_T^k on X_i , Φ_{square} is the square function, $\mathcal{F}_{AvgPool}$ is the average pooling operation, and Φ_{log} is the logarithmic function.

The output of all levels’ T kernels will be concatenated along the feature dimension. Hence, the output of the multi-scale temporal convolutional layer for X_i , $Z_{T-MS}^i \in \mathbb{R}^{t \times c \times \sum f_k}$, can be calculated by:

$$Z_{T-MS}^i = \Gamma(Z_{temporal}^1, \dots, Z_{temporal}^k) \quad (3)$$

where $\Gamma(\cdot)$ is the concatenation operation along the feature (f) dimension.

B. Graph Building Block

1) *Getting node attribute using Kernel-level attentive fusion*: After concatenation of the output from different level T kernels, a one-by-one convolutional layer is adopted as a kernel-level attentive fusion layer to fuse the features learned by different kernels. Batch normalization [41] is utilized before and after the one-by-one convolution to reduce the internal covariate shift effects. The number of one-by-one kernels is set as t . Leaky ReLU is utilized as the activation function. After that, an average pooling layer whose kernel is $(1, 2)$ is utilized to downsample the learned representations. After batch normalization, the fused representations from different one-by-one kernels are then flattened for each EEG channel as its node attribute in EEG-graph representation that will be introduced in the next section. This reshaping process is shown in Fig. 1 (b). Hence, the final temporal representation of each $X_i, Z_{T-fuse} \in \mathbb{R}^{c \times t \times 0.5 \times \sum f_k}$, is calculated by:

$$Z_{T-fuse}^i = \mathcal{F}_{reshape}(\mathcal{F}_{bn}(\mathcal{F}_{AvgPool}(\mathcal{F}_{fuse}(\mathcal{F}_{bn}(Z_{T-MS}^i))))) \quad (4)$$

where \mathcal{F}_{bn} is the batch normalization function, \mathcal{F}_{fuse} is the one-by-one convolution function, $\mathcal{F}_{AvgPool}$ is the average pooling operation, and the $\mathcal{F}_{reshape}$ is the reshape operation to build the attribute of each node (EEG channel) in the EEG graph representations.

2) *Defining local-global graphs of EEG*: In this section, three types of local-global-graph representations are constructed based on neuroscience findings [23][25][27], namely general local-global graph \mathcal{G}_g , frontal local-global graph \mathcal{G}_a , and hemisphere local-global graph \mathcal{G}_h . Given $Z_{T-fuse} \in \mathbb{R}^{c \times t \times 0.5 \times \sum f_k}$, each electrode is regarded as one node in the EEG graph, and the learned dynamic temporal representations of electrodes are regarded as the node attributes. To learn more information on graph data, the adjacent relations among nodes are very important. To effectively define adjacent relations, several neuroscience findings are taken into consideration.

Firstly, we define a general local-global graph. Human brains have several functional regions which will be active during different cognitive processes [23]. A well-known definition of functional regions is that the brain can be divided into the frontal lobe, parietal lobe, temporal lobe, and occipital lobe [18]. EEG collected from the electrodes located on the surface of the brain capture activities of different functional areas. They are placed according to the 10-20 system [18] that groups channels according to the location on different functional areas of the brain. We define the local graph based on the different functional areas of the brain according to the 10-20 system. The general local-global-graph definition, \mathcal{G}_g , is shown in Fig. 2 (a). LGGNet using the general local-global-graph definition is regarded as LGGNet-G and may be used for more generalized BCI classification tasks.

The frontal local-global graph is further defined based on several neuroscience findings on cognition and emotion studies. The frontal lobe is the largest portion of the brain, and it is responsible for high-level behaviours, such as thinking, attention, and emotions [23]. The frontal attention system is important in executive attentional control [42]. Distinguishable asymmetries exist across numerous nodes in the network

of brain areas involved in emotion, particularly within the frontal area [25]. The frontal asymmetries also reflect subjects' attentional bias to threat [43]. Hence, the frontal area is further split into several smaller local graphs which are symmetrically located on the left and right frontal hemispheres to learn more discriminative information. The frontal local-global graph, \mathcal{G}_f is shown in Fig. 2 (b).

For the hemisphere local-global graph, we adopt the definition in [44], which has symmetrical sub-graphs on the left and right hemispheres for all the functional areas. The hemisphere local-global graph, \mathcal{G}_h is shown in Fig. 2 (c).

After defining the local-global graphs, the local-global connections among them will be defined. The electrodes within one local graph are fully connected because we hypothesize that different electrodes within a sub-group can reflect the similar brain activities of the corresponding functional areas. The local adjacent matrix A_{local} is defined as:

$$A_{local} = \begin{bmatrix} 1 & \cdots & 1 \\ \vdots & \ddots & \vdots \\ 1 & \cdots & 1 \end{bmatrix} \quad (5)$$

where all elements are 1. The size of the A_{local} depends on how many channels are within the local graph.

The global connection is defined based on the relations among local graphs. Neuroscience studies suggested that activating one particular brain region also tends to activate other regions in the group for the high-level cognitive process [25]. Hence we hold the hypothesis that the local graphs are not independent during cognitive processes. The relations among local graphs are utilized as the edges in the global graph. Because the dot product of two vectors can measure the similarity between them, the dot products between local graph representations for each EEG instance are calculated to reflect the relations among local graphs. Note that, the similarity adjacent matrix is dynamic and instance-specific. We assume the global connection is undirected because the relation between two local graphs is mutual. Let \mathbf{h}_{local}^r be the latent representation of the r -th local graph. The adjacent matrix of the global graph, $A_{global} \in \mathbb{R}^{R \times R}$, where R is the total number of local graphs, is symmetric and can be defined as:

$$A_{global} = \begin{bmatrix} \mathbf{h}_{local}^1 \cdot \mathbf{h}_{local}^1 & \cdots & \mathbf{h}_{local}^1 \cdot \mathbf{h}_{local}^r \\ \vdots & \ddots & \vdots \\ \mathbf{h}_{local}^1 \cdot \mathbf{h}_{local}^r & \cdots & \mathbf{h}_{local}^r \cdot \mathbf{h}_{local}^r \end{bmatrix} \quad (6)$$

where \cdot is the dot product.

Due to the complex relations among brain functional areas, a trainable attentive mask is adapted to emphasize the most important connections in the instance-level similarity adjacent matrix. Note that the trainable mask is also symmetric because the global adjacent matrix is undirected. The trainable attentive mask, $\mathbf{M} \in \mathbb{R}^{R \times R}$, can be defined as:

$$\mathbf{M} = \begin{bmatrix} \mathbf{w}_{1,1} & \cdots & \mathbf{w}_{1,r} \\ \vdots & \ddots & \vdots \\ \mathbf{w}_{1,r} & \cdots & \mathbf{w}_{r,r} \end{bmatrix} \quad (7)$$

where \mathbf{w} are the trainable parameters.

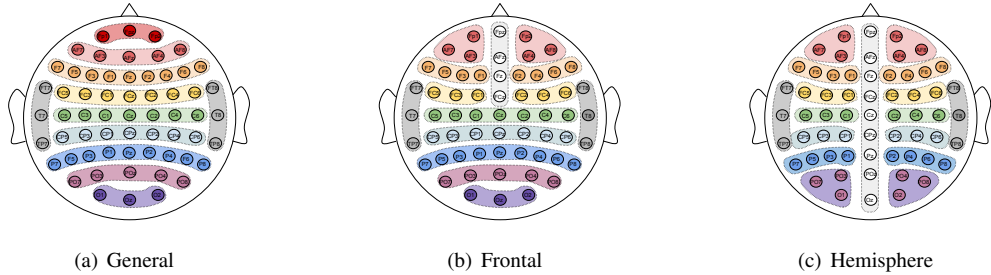


Fig. 2. Three types of local-global-graph definitions. (a) The general local-global-graph definition. This local graph structure is defined according to the 10-20 system. Each local graph reflects the brain activities of a certain brain functional area. (b) The frontal local-global-graph definition. Based on the general local-global graph, the neuroscience evidence of frontal asymmetry patterns in frontal areas is further considered. Six frontal local graphs that are symmetrically located on the left and right frontal areas of the brain are added to learn more discriminative information. (c) The hemisphere local-global-graph definition. The symmetrical local graphs are added for all the functional areas defined in the general local-global graph. The nodes in a local graph are in the same color. The dotted lines are the local graphs. This diagram illustrates the definition for the 62 channel EEG.

Self-loops are added after applying the trainable mask to the global adjacent matrix. Because adding self-loops after applying the trainable mask can maintain the strength of the self-loops since the value of the trainable mask is generally small. The ReLU activation function is applied to make the adjacent matrix non-negative. Hence the final global adjacent matrix can be calculated as:

$$A_{global} = \Phi_{ReLU}(A_{global} \circ M) + I \quad (8)$$

where \circ is the Hadamard product, and $I \in \mathbb{R}^{R \times R}$ is the identity matrix.

Having the node attributes, $Z_{T-fuse} \in \mathbb{R}^{c \times t \times 0.5 \times \sum f_k}$, and the adjacent matrix of the local-global graphs, graph filtering are designed to learn the local-global graph representations in the next two sections.

C. Graph Learning Block

1) *Local graph-filtering layer*: In order to learn the local brain activities, a local graph-filtering layer is proposed to attentively aggregate the learned representations within each local graph, $Z_{T-fuse} \in \mathbb{R}^{c \times t \times 0.5 \times \sum f_k}$. Local graphs reflect the brain activities of a certain functional area. Hence, the nodes in the local graph are fully connected. There are two steps in the local graph-filtering layer: Local graph filtering and local representation aggregating. Given the trainable local graph-filtering matrix $W_{local} \in \mathbb{R}^{c \times t \times 0.5 \times \sum f_k}$, and local graph-filtering bias vector $b_{local} \in \mathbb{R}^{c \times 1}$, the local graph-filtering weights will be assigned to the representation of each electrode by:

$$Z_{filtered}^i = \mathcal{F}_{AvgPool}(\Phi_{ReLU}(W_{local} \circ Z_{T-fuse}^i - b_{local})) \quad (9)$$

where \circ is the Hadamard product.

After local graph filtering, the attentively filtered representation within each local graph will be aggregated by an aggregating function $\mathcal{F}_{aggregate}(\cdot)$ to get the hidden embeddings of the local graphs. Let $Z_{filtered}^i = [Z_1^i, \dots, Z_r^i]^T$, $r \in [1, R]$ be the locally filtered graph representations, where $Z_r^i \in \mathbb{R}^{c' \times f'}$ is the local-graph representation, R is the total number of local graphs, c' is the number of nodes in the local graph ($\sum c_r' = c$), and f' is the feature length of each node

after local graph filtering. A local graph can be denoted as: $Z_r' = [z_1^1, \dots, z_r^p]^T$, $p \in [1, P_r]$, where z_r^p is the node vector in the local graph, and P_r is the total number of nodes in the r -th local graph. The aggregating function will aggregate the node vectors within each local graph. It can be maximum, minimum, average, etc. In LGGNet, the average operation is selected as the aggregating function. Hence, the output of the local graph-filtering layer, $Z_{local}^i \in \mathbb{R}^{R \times f'}$, where R is the total number of the local graphs, can be calculated by:

$$\begin{aligned} Z_{local}^i &= \mathcal{F}_{aggregate}(Z_{filtered}^i) \\ &= \mathcal{F}_{aggregate}([Z_1^i, \dots, Z_r^i]^T) \\ &= \left[\frac{1}{P_1} \sum_{p=1}^{P_1} z_1^p, \dots, \frac{1}{P_r} \sum_{p=1}^{P_r} z_r^p \right]^T \end{aligned} \quad (10)$$

where r is the index of local graphs, p is the index of nodes in each local graph, and P_r is the number of nodes in r -th local graph.

2) *Global graph-filtering layer*: The graph convolution on the global graph is designed to learn the complex relations among local graphs. The global graph represents the complex relations among different brain functional areas by the global adjacent patterns in the graph representations of EEG.

Given the global adjacent matrix, $A_{global} \in \mathbb{R}^{R \times R}$ described in Eq.8, the GCN [40] layer is adopted to learn the global-graph representations. The normalized adjacent matrix, \tilde{A}_{global} , can be calculated by:

$$\tilde{A}_{global} = \tilde{D}^{-\frac{1}{2}} A_{global} \tilde{D}^{-\frac{1}{2}} \quad (11)$$

where $\tilde{D} = \sum_q A_{global}^{p,q}$ is the degree matrix of the A_{global} . Let the nonlinear projecting weight matrix of m -th GCN layer be $W_m \in \mathbb{R}^{f' \times h}$, where h is the length of the hidden output after GCN, and the trainable bias vector be $b_m \in \mathbb{R}^{R \times 1}$. In the experiment, we found that subtracting bias before graph convolution had slightly better performance. Hence, the output of m -th GCN layer can be calculated as:

$$Z_m = \Phi_{ReLU}(\tilde{A}_{global}(Z_{m-1} W_m - b_m)) \quad (12)$$

where m is the index of GCN layers.

Before the global graph filtering, batch normalization, $\mathcal{F}_{bn}(\cdot)$, is applied to avoid internal covariant shift issue. In

LGGNet, the number of global GCN layers is set to be one. Let the nonlinear projecting weight matrix of GCN layer be $\mathbf{W}_{global} \in \mathbb{R}^{f' \times h}$, where h is the length of the hidden output after GCN, and the trainable bias vector be $\mathbf{b}_{global} \in \mathbb{R}^{R \times 1}$. The global-graph filtering of \mathbf{Z}_{local}^i can be calculated by:

$$\mathbf{Z}_{global}^i = \Phi_{ReLU}(\tilde{\mathbf{A}}_{global}(\mathcal{F}_{bn}(\mathbf{Z}_{local}^i)\mathbf{W}_{global} - \mathbf{b}_{global})) \quad (13)$$

After getting the globally filtered representation, batch normalization is applied. Then the flattened representation will be fed into a linear layer to generate the final classification output as:

$$Output = \Phi_{softmax}(\mathbf{W}\mathcal{F}_{dropout}(\Upsilon(\mathcal{F}_{bn}(\mathbf{Z}_{global}^i)))+\mathbf{b}) \quad (14)$$

where the $\Upsilon(\cdot)$ is the flatten operation, \mathbf{W} is the trainable weight matrix, and \mathbf{b} is the bias term.

Finally, the proposed LGGNet can be summarized in Algorithm 1

Algorithm 1: LGG

Input: EEG data $X_i \in \mathbb{R}^{c \times l}$; ground truth label y ; graph definitions \mathcal{G}_g , \mathcal{G}_f , and \mathcal{G}_h ; global adjacent matrix \mathbf{A}_{global}
Output: $pred$, the prediction of LGGNet

- 1 Initialization;
- 2 **for** $j \leftarrow 1$ **to** 3 **do**
- 3 get j -th temporal kernel size by **Eq. 1**;
- 4 get $\mathbf{Z}_{temporal}^j$ by **Eq. 2** using X_i as input;
- 5 **end**
- 6 get \mathbf{Z}_{T-MS}^i by **Eq. 3**;
- 7 do kernel-level attention fusion by **Eq. 4** to get \mathbf{Z}_{T-fuse}^i ;
- 8 do local filtering on each node attribute by **Eq. 9**;
- 9 aggregate the filtered node attribute within each local graph (\mathcal{G}_g , \mathcal{G}_f , or \mathcal{G}_h) by **Eq. 10**;
- 10 normalize the \mathbf{A}_{global} by **Eq. 11**;
- 11 do global filtering on embeddings of local graphs by **Eq. 13** with $\tilde{\mathbf{A}}_{global}$;
- 12 get $pred$ by **Eq. 14**;
- Return:** $pred$

IV. EXPERIMENTS

A. Datasets

Three publicly available datasets of different tasks are utilized to evaluate the proposed LGGNet: the attention dataset [29] for cognitive attention classification, the fatigue dataset [30] for mental fatigue classification, and the DEAP dataset [31] for emotion and preference classification, respectively.

The attention dataset is a multimodal brain-imaging dataset to measure three cognitive tasks of healthy subjects. It is available for download on this website¹. The EEG, and near-infrared spectroscopy (NIRS) were recorded while the subjects were doing three types of cognitive tasks: 1) n-back (0-, 2-, and 3-back), 2) discrimination/selection response task (DSR)

¹http://doc.ml.tu-berlin.de/simultaneous_EEG_NIRS/

and 3) word generation (WG) tasks. Only the DSR task was involved in this paper for cognitive attention classification. 26 subjects participated in the experiments. There were three sessions of the experiment for each subject. There were several series of attention task period (40s) and rest period (20s) in each session. To avoid the effects of cross-session variance, only the first session was utilized. The data were collected using a BrainAmp EEG amplifier with a sampling rate of 1KHz. 28 EEG channels and 2 electrooculographic (EOG) channels were recorded.

The fatigue dataset provides the EEG signals to measure the cognitive fatigue states of the driver during a 90-min-long driving task in a VR driving environment. It can be downloaded via this link². 27 subjects participated in the data collection experiments. The subjects were introduced to keep the car cruising in the center of the lane. Random lane-departure events were induced during the driving experiments. The subject needed to take action to make the car back to the center of the lane. Each trial included events with deviation onset, response onset, and response offset. The fatigue level of the subjects was measured by the reaction time of the sudden events. 32-channel EEG were collected with a sampling rate of 500Hz.

DEAP is a multi-modal human affective states dataset, including EEG, facial expressions, and galvanic skin response (GSR). The dataset is available on this website³. 40 emotional music videos are carefully selected as the stimuli to induce different emotions to the subject. Each video lasts for 1 min. Before each trial, there is a 3 seconds' baseline recording stage. An online self-assessment tool is designed to collect the feedback of subjects on arousal, valence, dominance, and liking. For each dimension, a continuous 9-point scale was adopted to measure the level of those dimensions. The valence and liking dimensions were utilized for the emotion and preference classification tasks in this paper. 32 subjects participated in the data collection experiments. During the experiment, EEG, GSR, and facial expressions are recorded. A 32-channel Biosemi ActiveTwo system was used with the sampling rate being 512 Hz.

B. Pre-processing

Deep learning can learn from EEG data directly instead of using human extracted features [14][11][21]. Hence, EEG data with several pre-processing operations are used as the input samples of the neural networks.

For the attention dataset, a band-pass filter from 0.5-50 Hz was applied to remove low and high-frequency noise as [17]. EOG was removed using the automatic ICA EOG removal method in the MNE toolbox [45]. Then the data were downsampled to 200 Hz to accelerate the training process. Following [46], only the first half of each attention trial was utilized to balance the samples between attention and inattention (rest). Each trial was further segmented into 4-second segments with a 50% overlap.

²<https://figshare.com/articles/dataset/MultichannelEEGrecordingsduringasustained-attentiondrivingtask/6427334>

³<http://www.eecs.qmul.ac.uk/mmv/datasets/deap/index.html>

TABLE II

COMPARISON BETWEEN OUR PROPOSED LGGNet AGAINST SOTA CLASSIFIERS ON THREE BENCHMARK DATASETS USING TRIAL-WISE N-FOLD CROSS-VALIDATION.

	Attention		Fatigue		Emotion		Preference	
model	mean ACC(%)	mean F1(%)						
DeepCN[11]	58.97*	64.30	66.86**	74.79**	58.67	57.48*	61.98	70.59
EEGNet[14]	58.05*	59.06	87.62	84.85	56.38	60.03**	58.41**	67.45***
R2G-STNN[32]	57.76*	57.99*	88.79**	88.42*	60.11	63.40	60.99**	69.89**
TSeption[21]	57.76*	57.93*	86.17**	84.77*	57.46**	60.42***	61.70*	70.34***
HRNN[17]	56.84*	55.20*	77.96*	72.76	58.46	60.93*	62.74	71.31*
LGGNet-H	61.22	60.08	89.83	89.14	58.85	64.15	63.07	72.53
LGGNet-F	63.07	60.63	90.76	90.18	58.80	63.68	62.86	71.96
LGGNet-G	64.53	64.40	90.14	89.31	59.19	64.51	62.86	72.42

p-value of the improvement of LGGNet over the method: * indicating ($p < 0.05$), ** indicating ($p < 0.01$), *** indicating ($p < 0.001$). LGGNet-H, LGGNet-F, LGGNet-G: LGGNet using hemisphere, frontal, and general local-global graphs.

For the fatigue dataset, the officially preprocessed EEG dataset [30] was used in this paper. Based on the original paper [30], the raw EEG signals were band-passed from 1 to 50 Hz to remove low and high-frequency noise. The authors manually removed the apparent eye blinks by visual checking. The Automatic Artifact Removal (AAR) method in EEGLab [47] was used to remove ocular and muscular artifacts. The processed data were downsampled to 128 Hz as [48]. For fatigue level calculation, we also followed [48]. The 3s' EEG data before the onset of the lane-departure events were used as EEG trials. Reaction time (RT) was utilized to measure the fatigue level for the EEG trials. RT was defined as the time from the onset of the lane-departure event to the onset of the counter-steering event. The RT of one trial was defined as local RT, denoted by RT_l . The global RT (RT_g) of the one trial was the mean of the local RTs of all the trials within a 90-second window before the current trial. The 5th percentile of all local RTs in the entire session was selected as an alert RT, RT_a . Let 0 be the label of fatigue class, and 1 be the non-fatigue class, the labeling process can be defined as:

$$y = \begin{cases} 0 & RT_l > 2.5 * RT_a \& RT_g > 2.5 * RT_a \\ 1 & RT_l < 1.5 * RT_a \& RT_g < 1.5 * RT_a \end{cases} \quad (15)$$

We follow [48], only the subjects whose number of the smaller class trial is larger than 50 was utilized for evaluation. However, we didn't balance the data as [48] did, so that more data is available to train the network and our proposed method is able to classify unbalanced data.

For DEAP, the processed data provided by the author was utilized. First, the 3 seconds' pre-trial baseline was removed from each trial. After that, the data were down-sampled to 128 Hz. EOG was removed using the method described in [31]. A band-pass filter was applied to remove the signals which were lower than 4 Hz and higher than 45 Hz. Average reference was conducted on the filtered data to get the final pre-processed data. The label for each dimension was a continuous 9-point scale. To divide each dimension into high/low classes, 5 was chosen as the threshold to project the 9 discrete values into low and high classes in each dimension as [31][49]. Each trial was further split into 4s shorter segments without overlap to train the neural network.

C. Evaluation Metrics

The accuracy and F1 score were used as the evaluation metrics. The reason for using accuracy is that it is one of the most commonly used evaluation metrics in classification problems. And F1 score was also utilized because it can provide a more comprehensive evaluation of the classifier when the data has unbalanced classes. For the fatigue and DEAP datasets, the classes are unbalanced. Hence, using both accuracy and F1 score can provide a better evaluation of the classifier. The calculating formulas of accuracy and F1 score are illustrated as follows:

$$Accuracy = \frac{TP + TN}{TP + FP + TN + FN} \quad (16)$$

$$F1 = \frac{TP}{TP + \frac{1}{2}(FP + FN)} \quad (17)$$

where TP is the true positive, TN is the true negative, and FP is the false positive, and FN is the false negative.

D. Experiment Settings

Trial-wise n-fold cross-validation for subject-specific experiments was adopted to evaluate the proposed LGGNet.

For the fatigue dataset and DEAP, all the trials of each subject were randomly divided into 10 folds. For the attention dataset, a trial-wise 6-fold cross-validation was adopted to balance the number of trials in each fold. Note that the random splitting is trial-wise to avoid potential data leakage issues for the attention and DEAP datasets since each trial is split into shorter segments as [21]. This step ensures that the highly correlated segments within a trial do not appear in both train and test data in a cross-validation fold. For the continuous cognitive processes in the brain, such as attention and emotion, the adjacent data segments in one trial are highly correlated. If one randomly shuffles the segments before the training-testing split, the highly correlated segments will appear in both training and test data, hence a very high classification result will be observed. However, the accuracy will drop when the highly correlated segments are never seen by the model in a real-world situation.

The nested cross-validation [50] was utilized to avoid biased evaluation. The outer loop of the nested cross-validation is

the trial-wise n-fold cross-validation, and the inner loop is another k-fold cross-validation, where $n_{DEAP} = n_{fatigue} = 10$, $n_{attention} = 6$, and $k = 3$ in this work. The average accuracy and F1 score of all subjects are reported as the final evaluation criterion as [31][49]. In the inner loop, to make full use of the training data, a two-stage training strategy is utilized as well, and more details about the two-stage training process will be provided in the next section.

E. Two-stage Training

To make full use of the training data, for each step of trial-wise n-fold cross-validation, the neural networks are trained in two stages using the training data. Since the inner loop of the nested cross-validation is the k-fold cross-validation, one fold of training data is utilized as validation data in each step of the k-fold cross-validation. First, the best-performing model in the k folds is saved as the candidate for testing. Then all k folds of the training data are combined as the new training data. The candidate model is fine-tuned on the combined training data with a smaller learning rate compared with the first stage training. In the second stage, the pre-trained model is trained for a maximum of 20 epochs. The training process stops when the training accuracy reaches 100% the first time to make sure the model is well fine-tuned without over-fitting. Test data is not used in any step of the two-stage model training. After getting the fine-tuned model, it will be evaluated on the test data.

F. Implementation Details

The code is implemented using PyTorch [51] library, and the source code can be found via this link⁴. For model training, the maximum training epoch of the first stage was 200 while the one for stage II was 20 instead. The batch size was 64. The dropout rate was set as 0.5 for all three datasets. Adam optimizer was utilized to optimize the training process with the initial learning rate being 1e-3 which was scaled down by 0.1 in the second stage. For the attention dataset, we used 1e-2 as the initial learning rate because it yielded higher validation accuracy. Early stopping was applied to reduce the training time and overcome over-fitting. Cross-entropy loss was selected as the loss function to guide the training process. We set the hidden size of GCN to 32 and the number of T kernels to 64 for all three datasets. We tuned the pooling size of the power layer on the attention dataset based on the performance on the validation set and applied the same value to the fatigue dataset. The pooling size and step of the power layer were 128 and $0.25*128 = 32$ for the attention and the fatigue dataset, the pooling size for DEAP was set as 16 since DEAP had more data that needed a deeper model to learn. Note the hyper-parameter settings were the same for all the subjects within each dataset. Label smoothing with a 0.1 smoothing rate was applied when training networks on DEAP dataset because the classes were highly unbalanced for some subjects. For more details, please refer to the open-access GitHub repository for LGGNet.

⁴<https://github.com/yi-ding-cs/LGG>

V. RESULTS AND DISCUSSION

To evaluate the proposed LGGNet, we tested it on three publicly available datasets for cognitive attention [17], mental fatigue [30], emotion, and preference [31] four different types of cognitive tasks. The performances were compared with five state-of-the-art (SOTA) methods in the BCI domain: (1) **DeepConvNet (2017)** [11]; (2) **EEGNet (2018)** [14]; (3) **R2G-STNN (2019)** [32]; (4) **TSception (2020)** [21]; (5) **HRNN (2021)** [17]. For fair comparisons, all the baseline methods used the optimal parameters suggested by their authors and we used the same training codes and settings as that of LGGNet.

In this section, We first show the accuracies and F1 scores against the SOTA methods with statistical analysis. Extensive analysis experiments were conducted to understand LGGNet better, including ablation studies and the effect of the local-global graphs. Then saliency maps were utilized to visualize the most informative region of the data identified by LGGNet. The learned adjacent matrixes were visualized to see what relations of the local graphs were learned by LGGNet.

A. Statistical Analysis

We first report the mean accuracy (ACC) and mean F1 score on the three benchmark datasets for four types of cognitive tasks (shown in Table II). The two-tailed Wilcoxon Signed-Rank Test was utilized for the statistical analysis on the attention dataset and DEAP, while paired T-test was used on the fatigue dataset because there were fewer subjects in the fatigue dataset.

1) *Attention Classification Task:* LGGNet-G achieves the highest classification results in most of the experiments, especially for the attention dataset, on which the improvements of accuracies are all statistically significant. LGGNet-G is 7.69% ($p < 0.05$) and 9.20% ($p < 0.05$) higher than HRNN in terms of ACC and F1 score on the attention dataset. A 6.77% ($p < 0.05$) improvement on accuracy and a 6.47% ($p < 0.05$) improvement on F1 score over TSception are achieved by LGGNet-G. The accuracy and F1 score of LGGNet-G are 6.77% ($p < 0.05$) and 6.41% ($p < 0.05$) higher than these of R2G-STNN. LGGNet-G has 6.48% ($p < 0.05$) and 5.34% ($p = 0.091$) higher accuracy and F1 score than EEGNet. DeepConvNet is 5.56% ($p < 0.05$) and 0.1% ($p = 0.928$) lower than LGGNet-G in terms of accuracy and F1 score, respectively.

2) *Fatigue Classification Task:* On the fatigue dataset, the best accuracy and F1 score are achieved by LGGNet-F with most of the improvements being statistically significant. LGGNet-F achieves 90.76% classification accuracy and 90.18% F1 score in fatigue detection tasks which are 12.80% ($p < 0.05$) and 17.24% ($p = 0.068$) higher than the ones of HRNN, and 4.59% ($p < 0.01$) and 5.41% ($p < 0.05$) higher than the ones of TSception. Compared with R2G-STNN, the improvement of LGGNet-F are 1.97% ($p < 0.01$) on accuracy and 1.76% ($p < 0.05$) on F1 score. EEGNet has a accuracy of 86.33% and a F1 score of 81.97% that are 3.14% ($p = 0.231$) and 5.33% ($p = 0.302$) lower than the ones of LGGNet-F. DeepConvNet has 23.9% ($p < 0.01$) and 15.39% ($p < 0.05$) lower accuracy and F1 score than LGGNet-F.

3) *Emotion Classification Task*: LGGNet-G still achieves the highest F1 score in the emotion classification task, while the best accuracy is achieved by R2G-STNN. The differences in accuracies on the DEAP dataset are less than the ones on the other datasets, but all the LGGNet variants achieve relatively larger improvements over the baselines. Among all the LGGNet variants, LGGNet-G has 3.58% ($p < 0.05$) and 4.09% ($p < 0.001$) higher F1 scores than HRNN and TSception. Compared with R2G-STNN, the F1 score is slightly improved by 1.1% using LGGNet-G. The improvements achieved by LGGNet-G over EEGNet are 2.81% ($p = 0.105$) on accuracy and 4.48% ($p < 0.01$) on F1 score. DeepConvNet achieves the lowest F1 score which is 7.03% ($p < 0.05$) lower than the ones of LGGNet-G.

4) *Preference Classification Task*: LGGNet-H achieves the highest accuracy and F1 score in the preference classification task instead of LGGNet-G. But the performance differences between LGGNet-H and LGGNet-G are not significant. LGGNet-H slightly improves the accuracy by 0.33% over HRNN and it achieves the 1.22% ($p < 0.05$) higher F1 score than HRNN. The accuracy and F1 score of LGGNet-H are all significantly higher than the ones of TSception, R2G-STNN, and EEGNet with statistical significances ($p < 0.05$).

TABLE III
RESULTS OF ABLATION STUDIES ON DEAP USING LGGNET-H

AF	L	G	ACC(%)	Changes(%)	F1(%)	Changes(%)
	✓	✓	60.95	-2.12	68.45	-4.08
✓		✓	60.93	-2.14	69.36	-3.17
✓	✓		59.06	-4.01	67.08	-5.45
✓	✓	✓	63.07	-	72.53	-

✓: Keep the component.

AF: Kernel-level attentive fusion. L: Local graph-filtering layer.

G: Global graph-filtering layer.

Changes: Compared with the original LGGNet-H.

B. Ablation Study

To better understand the contribution of the components in LGGNet, several ablation studies were conducted to understand: 1) the contribution of the kernel-level attentive fusion. 2) the contribution of the local graph filtering; 3) the contribution of the global graph filtering. DEAP dataset is utilized because there are more data and subjects compared to the other datasets. The ablation studies were conducted on the preference classification task because the performances were better than the ones for the emotion classification task using DEAP. Hence, LGGNet-H was utilized because it achieved the best classification results among the proposed methods. Each component was removed from the LGGNet-H model one by one. The new classification accuracies and the performance changes are reflected in Table III.

1) *The Contribution of The Kernel-level Attentive Fusion*: The kernel-level attentive fusion is utilized in the temporal convolutional layer to attentively fuse the learned temporal representations of different kernels. According to results shown in the first row of Table III, removing the kernel-level attentive fusion makes the accuracy drop from 63.07%

to 60.95%, decreasing by 2.12%. For the F1 score, it even drops more with the decrease being 4.08%. The results show the effectiveness of the kernel-level attentive fusion.

2) *The Contribution of The Local Graph Filtering*: The local graph-filtering layer learns from each local graph and outputs the embedding of each local graph. The local graph filtering is operated on each local graph. The learned embedding will become the node attribute in the global graph. To understand the contribution of the local graph-filtering layer, it was removed from LGGNet. In this case, each EEG channel is one node in the graph and the global adjacent matrix, $A_{global} \in \mathbb{R}^{c \times c}$, reflects the connection among all the nodes (c is the number of EEG electrodes).

According to the results are shown in the second row of Table III, after removing the local graph-filtering layer entirely, the accuracy drops from 63.07% to 60.93%, decreasing by 2.14%. For the F1 score, it drops by 3.17%. This indicates the importance of the local graph-filtering layer.

3) *The Contribution of The Global Graph Filtering*: In LGGNet, global graph filtering is utilized on the learned local-graph embeddings. It is designed to learn the complex relations among different functional areas of the brain during high-level cognitive processes [23]. It was removed from the LGGNet to analyze its importance to the classification performance. In this situation, only the local graph-filtering layer is kept to learn the spatial pattern of EEG. After getting the embeddings of local graphs, the latent representation was fed into fully connected layers without global graph filtering.

According to the third row of Table III, the accuracy and F1 score all dropped after removing the global graph-filtering layer. And the decreases are higher than the ones without the local graph-filtering layer. A 4.01% drop was observed for accuracy after discarding the global graph-filtering layer, while the one for the F1 score was 5.45%. The results show the contribution of the global graph filtering is larger than the one of local graph filtering in LGGNet.

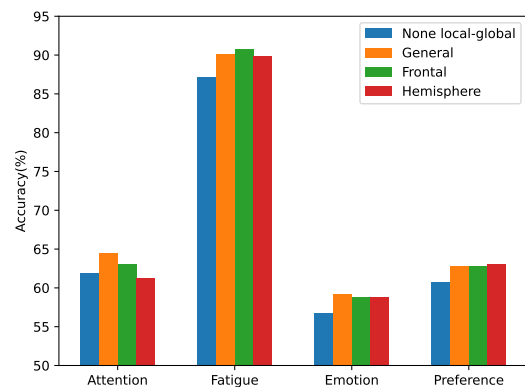


Fig. 3. Mean accuracies of LGGNet using different graph structures. The blue bar is the baseline that has no local-global graphs.

C. Effects of Local-Global Graphs

The success of LGGNet relies on well-defined local-global graphs. Prior knowledge of neuroscientific evidence is in-

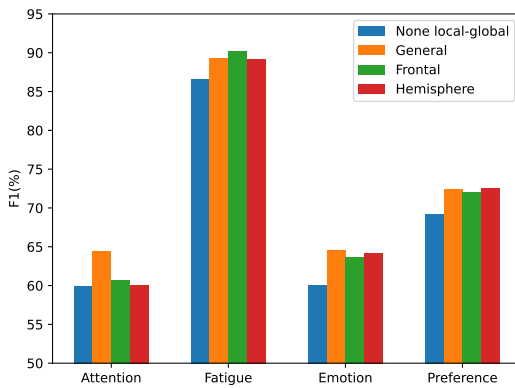


Fig. 4. Mean F1 scores of LGGNet using different graph structures. The blue bar is the baseline that has no local-global graphs.

volved in the graph structure design. To evaluate the effects of treating EEG as local-global graphs that were specially designed according to neuroscience, a none local-global graph was utilized as the baseline. Only global graph convolution was conducted because there were no local graphs in the baseline. The effects of different local-global-graph definitions were also analyzed by comparing their performances on different cognitive tasks. The results are shown in Fig. 3 and 4. And the detailed accuracies and F1 scores of three LGGNet variants are shown in the last three rows of Table II.

Using local-global graphs that are specially designed according to neuroscientific evidence yields significant improvements on classification performances for all four cognitive tasks, except the ones for the attention classification task when frontal and hemisphere local-global graphs were used in LGGNet. Compared with the baseline, LGGNet-G achieves 2.63% ($p = 0.087$) and 4.50% ($p < 0.05$) higher accuracy and F1 score than those of the baseline for the attention classification. For the fatigue detection task, the improvements achieved by using LGGNet-G are 2.99% ($p < 0.01$) and 2.75% ($p < 0.01$). In the emotion classification task, a 2.49% ($p < 0.001$) higher accuracy and a 4.48% ($p < 0.001$) higher F1 score are observed when the general local-global graph is used than the ones of the baseline that uses the none local-global graph. The improvements achieved by LGGNet-G on the preference classification task are 2.26% ($p < 0.01$) and 3.33% ($p < 0.001$) in terms of accuracy and F1 score. The results indicate the effectiveness of using local-global graphs to extract the spatial information of EEG.

The general local-global graph has a higher generalization ability as expected. LGGNet using the \mathcal{G}_g achieves the highest classification accuracies and F1 scores for both attention and emotion classification tasks. However, in the mental fatigue classification task, LGGNet-F achieves the highest F1 score and the highest accuracy. LGGNet-H achieves the highest classification results for the preference classification task instead. But the differences in performance are not significant for fatigue, emotion, and preference classification tasks. This suggests adding more symmetric local graphs in functional

areas can yield certain improvements over the general local-global graph for some tasks but the improvements are not significant.

D. Interpretability and Visualization

1) *Saliency Maps Visualization*: In this part, the saliency map [33] is utilized to visualize which parts of the data are more informative. To better visualize the saliency map, the original saliency map is averaged along the time dimension to get the topological map of the EEG channels for each subject. Fig. 5 shows the averaged saliency map of all the subjects.

From Fig. 5 (a), LGGNet mainly learns from frontal (Fp1, Fp2, F1, F2), temporal (T7 and T8), and parietal area (POz) of the brain for attention classification. This is also suggested in [42][52][53] that the frontal, temporal, and parietal lobes are attention-related regions.

The frontal area provides more fatigue classification-related information to LGGNet. According to Fig. 5 (b), strong activations are observed on Fp1, Fp2, F7, FC3 and FC4. This is consistent with other studies [54] which indicate the frontal lobe is related to human fatigue states.

From Fig. 5 (c), LGGNet learns more emotional information from the frontal (Fp2, AF4, and FC2) and temporal areas (T7 and T8) of the brain. The frontal area of the brain is full of emotional information [18][55]. The temporal lobe of the brain has relations to the emotional process [56].

According to Fig. 5 (d), LGGNet learns more from the temporal areas (T7 and T8) of the brain. Neuroimaging study [57] suggests the temporal lobes are predictive for the preference prediction during video watching, and these brain areas are related to sensory integration and emotional processing.

The above neurological knowledge indicates the neural network learns from the task-related regions of EEG signals.

2) *Learned Global Connection Visualization*: In this section, the learned adjacent matrixes of each task's best performing model are visualized to understand what relations LGGNet learns from EEG for different cognitive tasks. To get a general view of each cognitive task, the normalized adjacent matrixes are averaged for all the subjects. Because the adjacent relations are among local graphs instead of individual EEG channels, the names of the local graphs are defined by the name of the functional area. The 'l' and 'r' are utilized to indicate the location of the symmetric sub-graphs within a functional area. The values on the diagonal of the adjacent matrix reflect the proportions of each local graph embedding in the graph convolution operation, hence, they can serve as the attentive weights of the local graph embeddings. The other values show the strength of the relations among different local graphs.

Stronger correlations between frontal (AF, FC) and parietal (PO and P) regions are observed in Fig. 6 (a) for attention classification task. And for the self-connections, frontal (Fp), parietal (CP and P), and temporal (T-l and T-r) have higher attentive weights. This is consistent with [53] that indicates the posterior parietal lobe (PPL) that has dense connectivity with the cortical and subcortical regions in frontal, temporal, and occipital lobes. And it is important to attention function.

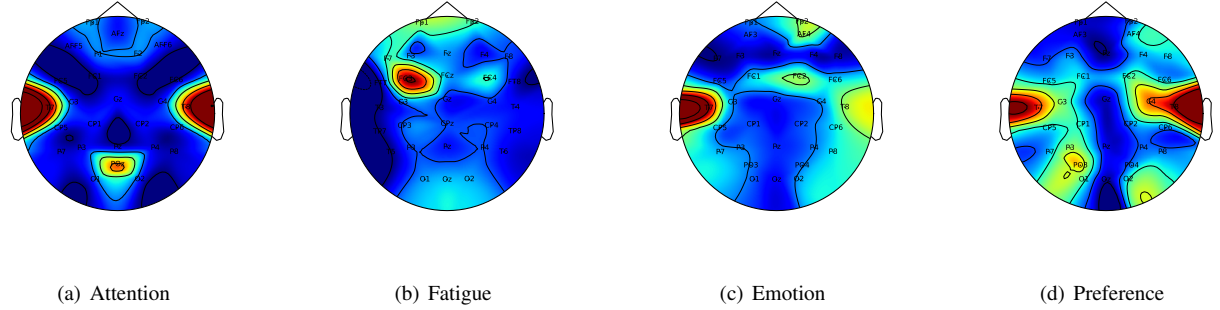


Fig. 5. Mean saliency maps of all subjects for three datasets. (a) is the mean saliency map for PhyDAA that is related to the cognitive attention classification task. (b) is the mean saliency map for the fatigue dataset that is related to mental fatigue classification. (c) is the mean saliency map for DEAP that is related to emotion classification.

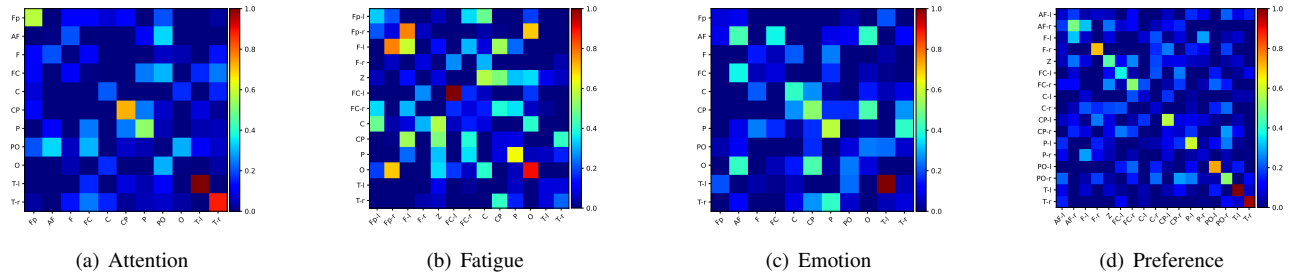


Fig. 6. Visualization of the learned adjacent matrixes for four cognitive tasks. (a) is the mean adjacent matrix for the attention classification task. (b) is the mean adjacent matrix for the fatigue dataset that is related to mental fatigue classification. (c) and (d) is the mean adjacent matrixes for DEAP that is related to the emotion and preference classification tasks.

According to Fig. 6 (b), stronger relations are observed among frontal sub-areas (Fp-r and F-l) for the fatigue classification task. The correlations between frontal and occipital areas (Fp-r and O), frontal and motor areas (F-l and CP, Fp-l and C) are also strong. For the self-connections, more attentive weights are given to frontal (Fp-l, F-l, and FC-l), parietal (P), and occipital (O). The frontal lobe and parietal areas are related to mental attention functions. The strong correlation among frontal, occipital, and motor areas may be because the visual and motor processes were involved in the fatigue experiment (driving in VR).

For the emotion classification task, more strong connections among frontal (AF and FC), occipital (O), and temporal (T-l, T-r) are shown in Fig. 6 (c) than the attention and preference classification tasks. This is also consistent with neuroscience [25] that the emotional process involves more basic processes, such as perception and attention. For self-connections, the frontal and temporal areas, commonly known as the emotion-related areas, have higher attention weights. However, C, CP, and P also get some attention weights, this may be caused by the attention function involved in the high-level emotional processes.

We find that there are fewer stronger relations among different local graphs in the learned adjacent matrix of the preference prediction task shown in Fig. 6 (d). More attentive weights are given to the temporal area (T-l, T-r) than the other regions. But the frontal (AF-r, F-r, FC-r) and occipital (PO-l and PO-r) contain PO and O channels in hemisphere local-global graph area are also highlighted.

Visualizing the learned adjacent matrixes shows the relations and the important local regions identified by LGGNet. And most of the learned relations are task-related. Since the cognitive processes are complex and may involve more basic processes that are not unique to the task, more analysis should be conducted in the future to better understand what and how the network learns from EEG.

Although LGG achieves the highest classification results for most of the experiments for four cognitive tasks, the limitation of this work should also be noticed. In this work, the nodes within each local area are set to be fully connected, which might not be able to reflect the complex brain activities inside that functional area. How to model the relations within local areas should be explored. Further improvement of the network or loss function design should be considered in the future to improve the classification performance.

VI. CONCLUSION

In this paper, we propose LGGNet, a neurologically inspired graph neural network, to learn from local-global-graph representations of EEG. Multi-scale 1D temporal convolutional kernels with kernel-level attention fusion are utilized to learn the temporal dynamics of EEG. Local and global graph filtering learn the brain activities within each functional area and the complex relations among them during the cognitive process in the brain, respectively. With a robust nested cross-validation strategy, the proposed method and several state-of-the-art methods are evaluated on three publicly available

benchmark datasets for attention, fatigue, emotion, and preference classification tasks. The proposed method achieves significantly ($p < 0.05$) higher accuracies and F1 scores than other methods in most of the experiments. Further analyses also show that applying neuropsychological knowledge to the network design ensures that networks are trained on task-specific neural activations.

ACKNOWLEDGMENT

This work was partially supported by the RIE2020 AME Programmatic Fund, Singapore (No. A20G8b0102). The authors would like to thank Mr. Chengxuan Tong for his help on code checking and Ms. Aidi Liu for her help on the proofreading of the manuscript.

REFERENCES

- [1] X. Zhang, J. Liu, J. Shen, S. Li, K. Hou, B. Hu, J. Gao, T. Zhang, and B. Hu, "Emotion recognition from multimodal physiological signals using a regularized deep fusion of kernel machine," *IEEE Transactions on Cybernetics*, pp. 1–14, 2020.
- [2] F. Lotte and C. Guan, "Regularizing common spatial patterns to improve BCI designs: unified theory and new algorithms," *IEEE Transactions on biomedical Engineering*, vol. 58, no. 2, pp. 355–362, 2010.
- [3] R. Liu, Y.-X. Wang, and L. Zhang, "An FDES-based shared control method for asynchronous brain-actuated robot," *IEEE Transactions on Cybernetics*, vol. 46, no. 6, pp. 1452–1462, 2015.
- [4] R. Foong, K. K. Ang, C. Quek, C. Guan, K. S. Phua, C. W. K. Kuah, V. A. Deshmukh, L. H. L. Yam, D. K. Rajeswaran, N. Tang *et al.*, "Assessment of the efficacy of eeg-based MI-BCI with visual feedback and EEG correlates of mental fatigue for upper-limb stroke rehabilitation," *IEEE Transactions on Biomedical Engineering*, vol. 67, no. 3, pp. 786–795, 2019.
- [5] V. Zotev, A. Mayeli, M. Misaki, and J. Bodurka, "Emotion self-regulation training in major depressive disorder using simultaneous real-time fMRI and EEG neurofeedback," *NeuroImage: Clinical*, vol. 27, p. 102331, 2020.
- [6] J. K. Carpenter, L. A. Andrews, S. M. Witcraft, M. B. Powers, J. A. J. Smits, and S. G. Hofmann, "Cognitive behavioral therapy for anxiety and related disorders: A meta-analysis of randomized placebo-controlled trials," *Depression and Anxiety*, vol. 35, no. 6, pp. 502–514, 2018.
- [7] Kai Keng Ang, Zheng Yang Chin, Haihong Zhang, and Cuntai Guan, "Filter bank common spatial pattern (FBCSP) in brain-computer interface," in *2008 IEEE International Joint Conference on Neural Networks (IEEE World Congress on Computational Intelligence)*, June 2008, pp. 2390–2397.
- [8] Y.-K. Wang, T.-P. Jung, and C.-T. Lin, "EEG-based attention tracking during distracted driving," *IEEE Transactions on Neural Systems and Rehabilitation Engineering*, vol. 23, no. 6, pp. 1085–1094, 2015.
- [9] W. Zheng, J. Zhu, and B. Lu, "Identifying stable patterns over time for emotion recognition from EEG," *IEEE Transactions on Affective Computing*, vol. 10, no. 3, pp. 417–429, July 2019.
- [10] P. Li, H. Liu, Y. Si, C. Li, F. Li, X. Zhu, X. Huang, Y. Zeng, D. Yao, Y. Zhang, and P. Xu, "EEG based emotion recognition by combining functional connectivity network and local activations," *IEEE Transactions on Biomedical Engineering*, vol. 66, no. 10, pp. 2869–2881, Oct 2019.
- [11] R. T. Schirrmeister, J. T. Springenberg, L. D. J. Fiederer, M. Glasstetter, K. Eggensperger, M. Tangermann, F. Hutter, W. Burgard, and T. Ball, "Deep learning with convolutional neural networks for EEG decoding and visualization," *Human Brain Mapping*, vol. 38, no. 11, pp. 5391–5420, 2017.
- [12] O.-Y. Kwon, M.-H. Lee, C. Guan, and S.-W. Lee, "Subject-independent brain-computer interfaces based on deep convolutional neural networks," *IEEE Transactions on Neural Networks and Learning Systems*, vol. 31, no. 10, pp. 3839–3852, 2020.
- [13] Y. R. Tabar and U. Halici, "A novel deep learning approach for classification of EEG motor imagery signals," *Journal of Neural Engineering*, vol. 14, no. 1, p. 016003, nov 2016.
- [14] V. J. Lawhern, A. J. Solon, N. R. Waytowich, S. M. Gordon, C. P. Hung, and B. J. Lance, "EEGNet: a compact convolutional neural network for EEG-based brain-computer interfaces," *Journal of Neural Engineering*, vol. 15, no. 5, p. 056013, Jul 2018.
- [15] F. Fahimi, Z. Zhang, W. B. Goh, T.-S. Lee, K. K. Ang, and C. Guan, "Inter-subject transfer learning with an end-to-end deep convolutional neural network for EEG-based BCI," *Journal of Neural Engineering*, vol. 16, no. 2, p. 026007, Jan 2019.
- [16] H. Cai, J. Tang, Y. Wu, M. Xia, G. He, and Y. Zhang, "The detection of attentive mental state using a mixed neural network model," in *2021 IEEE International Symposium on Circuits and Systems (ISCAS)*, 2021, pp. 1–5.
- [17] V. Delvigne, H. Wannous, T. Dutoit, L. Ris, and J.-P. Vandeborre, "PhyDAA: Physiological dataset assessing attention," *IEEE Transactions on Circuits and Systems for Video Technology*, pp. 1–1, 2021.
- [18] S. M. Alarcão and M. J. Fonseca, "Emotions recognition using EEG signals: A survey," *IEEE Transactions on Affective Computing*, vol. 10, no. 3, pp. 374–393, July 2019.
- [19] J. Li, Z. Zhang, and H. He, "Hierarchical convolutional neural networks for EEG-based emotion recognition," *Cognitive Computation*, vol. 10, no. 2, pp. 368–380, Apr 2018.
- [20] Y. Li, W. Zheng, Y. Zong, Z. Cui, T. Zhang, and X. Zhou, "A bi-hemisphere domain adversarial neural network model for EEG emotion recognition," *IEEE Transactions on Affective Computing*, vol. 12, no. 2, pp. 494–504, 2021.
- [21] Y. Ding, N. Robinson, Q. Zeng, D. Chen, A. A. Phylo Wai, T. S. Lee, and C. Guan, "TSception: a deep learning framework for emotion detection using EEG," in *2020 International Joint Conference on Neural Networks (IJCNN)*, 2020, pp. 1–7.
- [22] Z. Jiao, X. Gao, Y. Wang, J. Li, and H. Xu, "Deep convolutional neural networks for mental load classification based on EEG data," *Pattern Recognition*, vol. 76, pp. 582 – 595, 2018.
- [23] J. Power, A. Cohen, S. Nelson, G. Wig, K. Barnes, J. Church, A. Vogel, T. Laumann, F. Miezin, B. Schlaggar, and S. Petersen, "Functional network organization of the human brain," *Neuron*, vol. 72, no. 4, pp. 665 – 678, 2011.
- [24] A. D. Friederici, N. Chomsky, R. C. Berwick, A. Moro, and J. J. Bolhuis, "Language, mind and brain," *Nature Human Behaviour*, vol. 1, no. 10, pp. 713–722, 2017.
- [25] H. Kober, L. F. Barrett, J. Joseph, E. Bliss-Moreau, K. Lindquist, and T. D. Wager, "Functional grouping and cortical–subcortical interactions in emotion: A meta-analysis of neuroimaging studies," *NeuroImage*, vol. 42, no. 2, pp. 998 – 1031, 2008.
- [26] R. Mane, N. Robinson, A. P. Vinod, S.-W. Lee, and C. Guan, "A multi-view CNN with novel variance layer for motor imagery brain computer interface," in *2020 42nd Annual International Conference of the IEEE Engineering in Medicine Biology Society (EMBC)*, 2020, pp. 2950–2953.
- [27] J. J. B. Allen, P. M. Keune, M. Schönenberg, and R. Nusslock, "Frontal EEG alpha asymmetry and emotion: From neural underpinnings and methodological considerations to psychopathology and social cognition," *Psychophysiology*, vol. 55, no. 1, p. e13028, 2018.
- [28] T. Song, W. Zheng, P. Song, and Z. Cui, "EEG emotion recognition using dynamical graph convolutional neural networks," *IEEE Transactions on Affective Computing*, vol. 11, no. 3, pp. 532–541, 2020.
- [29] J. Shin, A. von Lühmann, D.-W. Kim, J. Mehnert, H.-J. Hwang, and K.-R. Müller, "Simultaneous acquisition of EEG and NIRS during cognitive tasks for an open access dataset," *Scientific Data*, vol. 5, no. 1, p. 180003, 2018.
- [30] Z. Cao, C.-H. Chuang, J.-K. King, and C.-T. Lin, "Multi-channel EEG recordings during a sustained-attention driving task," *Scientific data*, vol. 6, no. 1, pp. 1–8, 2019.
- [31] S. Koelstra, C. Muhl, M. Soleymani, J. Lee, A. Yazdani, T. Ebrahimi, T. Pun, A. Nijholt, and I. Patras, "DEAP: A database for emotion analysis using physiological signals," *IEEE Transactions on Affective Computing*, vol. 3, no. 1, pp. 18–31, 2012.
- [32] Y. Li, W. Zheng, L. Wang, Y. Zong, and Z. Cui, "From regional to global brain: A novel hierarchical spatial-temporal neural network model for EEG emotion recognition," *IEEE Transactions on Affective Computing*, pp. 1–1, 2019.
- [33] K. Simonyan, A. Vedaldi, and A. Zisserman, "Deep inside convolutional networks: Visualising image classification models and saliency maps," *arXiv preprint arXiv:1312.6034*, 2013.
- [34] N. Robinson, S. Lee, and C. Guan, "EEG representation in deep convolutional neural networks for classification of motor imagery," in *2019 IEEE International Conference on Systems, Man and Cybernetics (SMC)*, Oct 2019, pp. 1322–1326.

- [35] S. Siddharth, T. Jung, and T. J. Sejnowski, "Utilizing deep learning towards multi-modal bio-sensing and vision-based affective computing," *IEEE Transactions on Affective Computing*, pp. 1–1, 2019.
- [36] S. Jang, S. Moon, and J. Lee, "EEG-based video identification using graph signal modeling and graph convolutional neural network," in *2018 IEEE International Conference on Acoustics, Speech and Signal Processing (ICASSP)*, 2018, pp. 3066–3070.
- [37] P. Zhong, D. Wang, and C. Miao, "EEG-based emotion recognition using regularized graph neural networks," *IEEE Transactions on Affective Computing*, pp. 1–1, 2020.
- [38] F. Scarselli, M. Gori, A. C. Tsoi, M. Hagenbuchner, and G. Monfardini, "The graph neural network model," *IEEE Transactions on Neural Networks*, vol. 20, no. 1, pp. 61–80, Jan 2009.
- [39] M. Defferrard, X. Bresson, and P. Vandergheynst, "Convolutional neural networks on graphs with fast localized spectral filtering," in *Advances in Neural Information Processing Systems 29*, 2016, pp. 3844–3852.
- [40] T. N. Kipf and M. Welling, "Semi-supervised classification with graph convolutional networks," *Proc. of ICLR*, 2017.
- [41] S. Ioffe and C. Szegedy, "Batch normalization: Accelerating deep network training by reducing internal covariate shift," in *Proceedings of the 32nd International Conference on Machine Learning*, vol. 37, 07–09 Jul 2015, pp. 448–456.
- [42] T. Egner, G. Jamieson, and J. Gruzelier, "Hypnosis decouples cognitive control from conflict monitoring processes of the frontal lobe," *NeuroImage*, vol. 27, no. 4, pp. 969–978, 2005.
- [43] G. M. Grimshaw, J. J. Foster, and P. M. Corballis, "Frontal and parietal EEG asymmetries interact to predict attentional bias to threat," *Brain and Cognition*, vol. 90, pp. 76–86, 2014.
- [44] R. Grabner and B. De Smedt, "Oscillatory EEG correlates of arithmetic strategies: A training study," *Frontiers in Psychology*, vol. 3, p. 428, 2012.
- [45] A. Gramfort, M. Luessi, E. Larson, D. A. Engemann, D. Strohmeier, C. Brodbeck, L. Parkkonen, and M. S. Hämäläinen, "MNE software for processing MEG and EEG data," *NeuroImage*, vol. 86, pp. 446 – 460, 2014.
- [46] Y. Zhang, H. Cai, L. Nie, P. Xu, S. Zhao, and C. Guan, "An end-to-end 3D convolutional neural network for decoding attentive mental state," *Neural Networks*, vol. 144, pp. 129–137, 2021.
- [47] A. Delorme and S. Makeig, "EEGLAB: an open source toolbox for analysis of single-trial EEG dynamics including independent component analysis," *Journal of Neuroscience Methods*, vol. 134, no. 1, pp. 9–21, 2004.
- [48] Y. Liu, Z. Lan, J. Cui, O. Sourina, and W. Müller-Wittig, "EEG-based cross-subject mental fatigue recognition," in *2019 International Conference on Cyberworlds (CW)*, 2019, pp. 247–252.
- [49] A. Appriou, A. Cichocki, and F. Lotte, "Modern machine-learning algorithms: For classifying cognitive and affective states from electroencephalography signals," *IEEE Systems, Man, and Cybernetics Magazine*, vol. 6, no. 3, pp. 29–38, 2020.
- [50] S. Varma and R. Simon, "Bias in error estimation when using cross-validation for model selection," *BMC Bioinformatics*, vol. 7, no. 1, p. 91, 2006.
- [51] A. Paszke, S. Gross, F. Massa, A. Lerer, J. Bradbury, G. Chanan, T. Killeen, Z. Lin, N. Gimelshein, L. Antiga, A. Desmaison, A. Kopf, E. Yang, Z. DeVito, M. Raison, A. Tejani, S. Chilamkurthy, B. Steiner, L. Fang, J. Bai, and S. Chintala, "PyTorch: An imperative style, high-performance deep learning library," in *Advances in Neural Information Processing Systems 32*, 2019, pp. 8024–8035.
- [52] E. H. Kozasa, J. B. Balardin, J. R. Sato, K. T. Chaim, S. S. Lacerda, J. Radvany, L. E. A. M. Mello, and E. Amaro Jr., "Effects of a 7-day meditation retreat on the brain function of meditators and non-meditators during an attention task," *Frontiers in Human Neuroscience*, vol. 12, p. 222, 2018.
- [53] X. Yin, L. Zhao, J. Xu, A. C. Evans, L. Fan, H. Ge, Y. Tang, B. Khundrakpam, J. Wang, and S. Liu, "Anatomical substrates of the alerting, orienting and executive control components of attention: Focus on the posterior parietal lobe," *PLOS ONE*, vol. 7, no. 11, pp. 1–9, 11 2012.
- [54] D. Jing, D. Liu, S. Zhang, and Z. Guo, "Fatigue driving detection method based on EEG analysis in low-voltage and hypoxia plateau environment," *International Journal of Transportation Science and Technology*, vol. 9, no. 4, pp. 366–376, 2020.
- [55] P. A. Kragel, M. Kano, L. Van Oudenhove, H. G. Ly, P. Dupont, A. Rubio, C. Delon-Martin, B. L. Bonaz, S. B. Manuck, P. J. Gianaros *et al.*, "Generalizable representations of pain, cognitive control, and negative emotion in medial frontal cortex," *Nature neuroscience*, vol. 21, no. 2, pp. 283–289, 2018.
- [56] I. R. Olson, A. Plotzker, and Y. Ezzyat, "The enigmatic temporal pole: a review of findings on social and emotional processing," *Brain*, vol. 130, no. 7, pp. 1718–1731, 2007.
- [57] H.-Y. Chan, A. Smidts, V. C. Schoots, R. C. Dietvorst, and M. A. Boksem, "Neural similarity at temporal lobe and cerebellum predicts out-of-sample preference and recall for video stimuli," *NeuroImage*, vol. 197, pp. 391–401, 2019.